Long-distance indoor optical camera communication using side-emitting fibers as distributed transmitters

KLÁRA EÖLLŐS-JAROŠÍKOVÁ,[1,*] VOJTĚCH NEUMAN,[1] CRISTO MANUEL JURADO-VERDÚ,[2] SHIVANI RAJENDRA TELI,[1] STANISLAV ZVÁNOVEC,[1] AND MATĚJ KOMANEC[1]

[1]*Department of Electromagnetic Field, Faculty of Electrical Engineering, Czech Technical University in Prague, Technická 2, 166 27 Prague, Czech Republic*
[2]*Institute for Technological Development and Innovation in Communications, University of Las Palmas de Gran Canaria, Calle Practicante Ignacio Rodríguez, 35017 Las Palmas de Gran Canaria, Spain*
*eollokla@fel.cvut.cz

Abstract: We present a design approach for a long-distance optical camera communication (OCC) system using side-emitting fibers as distributed transmitters. We demonstrate our approach feasibility by increasing the transmission distance by two orders up to 40 m compared to previous works. Furthermore, we explore the effect of the light-emitting diode (LED) modulation frequency and rolling shutter camera exposure time on inter-symbol interference and its effective mitigation. Our proposed OCC-fiber link meets the forward-error-correction (FEC) limit of $3.8 \cdot 10^{-3}$ of bit error rate (BER) for up to 35 m (with BER= $3.35 \cdot 10^{-3}$) and 40 m (with BER=$1.13 \cdot 10^{-3}$) using 2-mm and 3-mm diameter side-emitting fibers, respectively. Our results at on-off keying modulation frequencies of 3.54 kHz and 5.28 kHz pave the way to moderate-distance outdoor and long-distance indoor highly-reliable applications in the Internet of Things and OCC using side-emitting fiber-based distributed transmitters.

1.   Introduction

Optical camera communication (OCC) has been evolving rapidly over the last few years, showing achievements in terms of illumination, communication, and localization functionalities within a range of applications such as indoor Internet of Things (IoT) based sensor networks and smart environments (homes, offices, and cities) [1,2]. In conventional OCC, a signal from a modulated light source, typically a light-emitting diode (LED), is captured in the form of a set of images or a video by using a rolling shutter (RS) camera [3]. The transmitted data are contained in the form of light and dark stripes depicting signal levels as a part of the captured image set.

Considering achieved link distances, [4] demonstrates several techniques to improve the transmission range from 10 m to 60 m. The listed techniques were a combination of under-sampled phase-shift on-off keying (UPSOOK), wavelength-division multiplexing (WDM), and multiple-input–multiple-output (MIMO) implemented on a red, green, and blue LED-based OCC channel. Outdoor long-distance OCC ranging from 60 m to 400 m transmission span for vehicle-to-vehicle and vehicle-to-infrastructure communication was reported in [5,6] using stereo camera-based distance measurement and convolutional neural network to optimize the source detection and recognition and camera defocusing techniques. These breakthroughs were based on the conventional OCC systems that utilize standard LEDs for data transmission and illumination purposes.

One major limitation of the above-mentioned configurations is the LED radiation pattern limiting the field-of-view (FOV) to 120°, along with the fact that an LED can be considered a point source. The point source limitation can be overcome using an LED strip or an LED

panel [7], which can be covered in a diffuser to create smoother light [8,9]. However, an LED strip or LED panel still does not have a 360° radiation pattern. As an alternative, side-emitting fibers (often also denoted as illuminating optical fibers or light-diffusing fibers) provide a 360° radiation pattern, and, moreover, they can transmit signal along the whole fiber length.

Side-emitting optical fibers are specially designed to gradually emit light along the fiber length, which is opposed to conventional optical fibers, where the primary purpose is to guide as much power as possible from one end fiber to the other. This side-emission effect, described as glowstick-like, decreases exponentially alongside the fiber length and may be achieved using multiple approaches, which vary according to the material composition of the side-emitting fiber [10]. In silica-based side-emitting fibers, the presence of nanovoids in the fiber core served to scatter light to the cladding and then emit along the fiber [11]. Similarly, particle-modified cladding silica side-emitting fiber was reported in [12]. The main parameter of side-emitting fibers is the diffusion length (*DL*) which defines the fiber length over which 90% of the optical signal power is lost, e.g., for *DL* = 1 m, we will get 10% of the coupled light at the output of 1-m-long side-emitting fiber [13]. The other parameters are the spectral transmission of the side-emitting fiber, which generally covers the whole visible region; the fiber diameter which is critical for OCC performance and fiber flexibility; and fiber material (glass or plastic).

The progress in side-emitting fibers has led to a number of possible applications of side-emitting fibers, such as door frame illumination, advertisement purposes, escape exit indicators, or transmitting location-specific information. Reports on the use of side-emitting fibers in fabrics for design purposes and sensing [14] and for microalgae growth [15] were presented.

Furthermore, side-emitting optical fibers were used as a spatially multiplexed light source within OCC in [16]. An extended use of side-emitting fibers as a distributed source has recently been proposed for OCC by our group [17] with a maximum link distance of 75 cm [18], whereas the distance of 35 cm was presented in [19] using a laser source, instead of an LED, coupled to the side-emitting fiber. Recently a study on side-emitting fibers in OCC was published, claiming a transmission distance of 23 m with bit error rate (BER) below the forward-error-correction (FEC) limit [20]. A long-short-term-memory neural network (LSTM-NN) processing approach and a telescope were employed in [20] to boost the transmission distance. Moreover, theoretical studies were published focusing on modeling and validating of power coupling into side-emitting fiber and its radiation [10,21].

In this paper, we present a new approach to OCC using side-emitting fibers as distributed transmitters, which brings unprecedented distance increase by more than two orders compared to previous results [17,19] (and almost double transmission distance published in [20], which uses a more complex and less reliable data processing technique of LSTM-NN). We achieve this significant transmission distance increase by employing a new method of exposure time and LED modulation frequency optimization accompanied by a reworked data processing routine. In comparison to [20], which employs the LSTM-NN processing, we use the matched filtering method as matched filtering is a fast-processing method and needs only a limited amount of information for perfect data processing, whereas LSTM-NN uses previous data samples to process the current data sample, thus the LSTM-NN system is very sensitive to slight deviations in the sampling clock. Therefore, the transmission distance presented in this paper is close to double of [20] but has the significant advantage of more reliable data processing.

We show that by using only 3 mm diameter side-emitting fiber, we can reach a transmission distance of up to 40 m with an LED modulation frequency above 5 kHz once employing our new approach using optimized data generation and processing. Results presented in this paper demonstrate that OCC using side-emitting fibers as distributed transmitters can be used for both long-distance indoor and mid-range outdoor communication, IoT, or sensory networks.

2. System design optimization

The following sections discuss the OCC link design using side-emitting fibers as distributed transmitters. We start with the RS camera settings, which define the essential parameters of our new side-emitting fiber-based OCC concept. Then we focus on the processing of captured data.

2.1. Exposure time and sampling period

In RS cameras, one row of pixels is exposed during an exposure time t_{exp}. The time period between the activation of two consecutive rows corresponds to the sampling period T_{s} [22]. The sampling period T_{s} is an intrinsic property of RS cameras and can also be presented as row sampling time or sampling rate f_{s}. The exposure time t_{exp} generally spans over multiple sampling periods T_{s}. The exposure time is either set manually by the user or is set automatically in dependence on the ambient light level. The impact of both parameters of T_{s} and t_{exp} on the overall OCC link performance is significant and will be explained in the following paragraphs.

When a long t_{exp} is used (Fig. 1(a)), the image sensor captures light for a period of time in which the transmitted symbol changes (from logical 1 to logical 0, or vice versa). The pixel is illuminated both with logical 0 and with logical 1 resulting in inter-symbol interference (ISI), implying that a long t_{exp} is unsuitable for OCC. The effect and the absence of the ISI in an image are illustrated in Fig. 1(a) and Fig. 1(b), respectively, by gray-scale bars in the right part of the image, where the result of each pixel illumination is integrated. When a short (proper) t_{exp} is used (Fig. 1(b)), each pixel is illuminated only for a short period of time, minimizing the ISI and thus generating a much clearer image. This tells us that to avoid significant ISI, the exposure time cannot be arbitrary, as with increased t_{exp} pixels integrate light over more time and the irradiance of several consecutive symbols might be captured on the same pixels during the exposition. Therefore, t_{exp} acts as a low-pass filter [22,23].
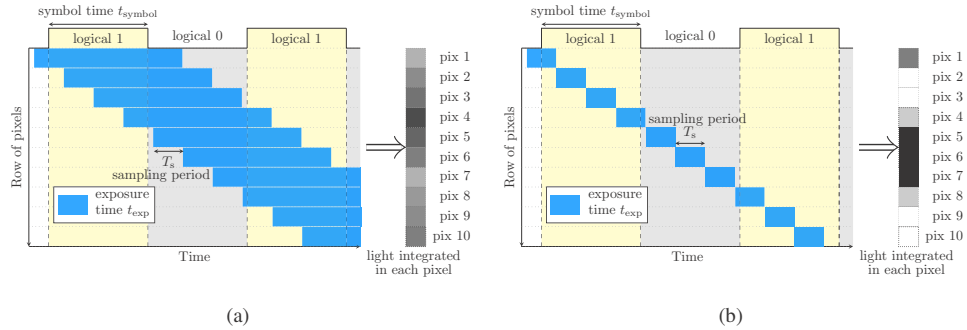
Fig. 1. Different exposure times in a rolling shutter camera can either (a) deepen the presence of inter-symbol interference (long exposure time), or (b) minimize it (short exposure time).

To efficiently suppress the effect of ISI, the exposure time t_{exp} must comply

$$t_{\text{exp}} \leq \frac{t_{\text{symbol}}}{2}, \tag{1}$$

where t_{symbol} is the symbol duration, i.e., the time the RS camera needs to capture one logical bit. The t_{symbol} is defined as

$$t_{\text{symbol}} = N_{\text{pps}} \cdot T_{\text{s}} = \frac{1}{f_{\text{Tx}}}, \tag{2}$$

where N_{pps} is the theoretically expected number of pixel rows (samples) per symbol, e.g., $N_{\text{pps}} = 10$, 15, or 20 px/symbol (pps). This means that we can choose what N_{pps} we want by selecting the t_{symbol} according to the RS camera sampling period T_{s}. Furthermore, the t_{symbol} translates

into modulation frequency f_{Tx} of the data signal to the LED transmitter as an inverse proportion. Previous statements imply the trade-off between t_{exp} and N_{pps}, and thus between data throughput and received signal magnitude. In the case of low-light conditions, the received signal quality might be improved by increasing the analog gain of the RS camera [24,25]. This can also significantly improve the signal-to-noise ratio (SNR).
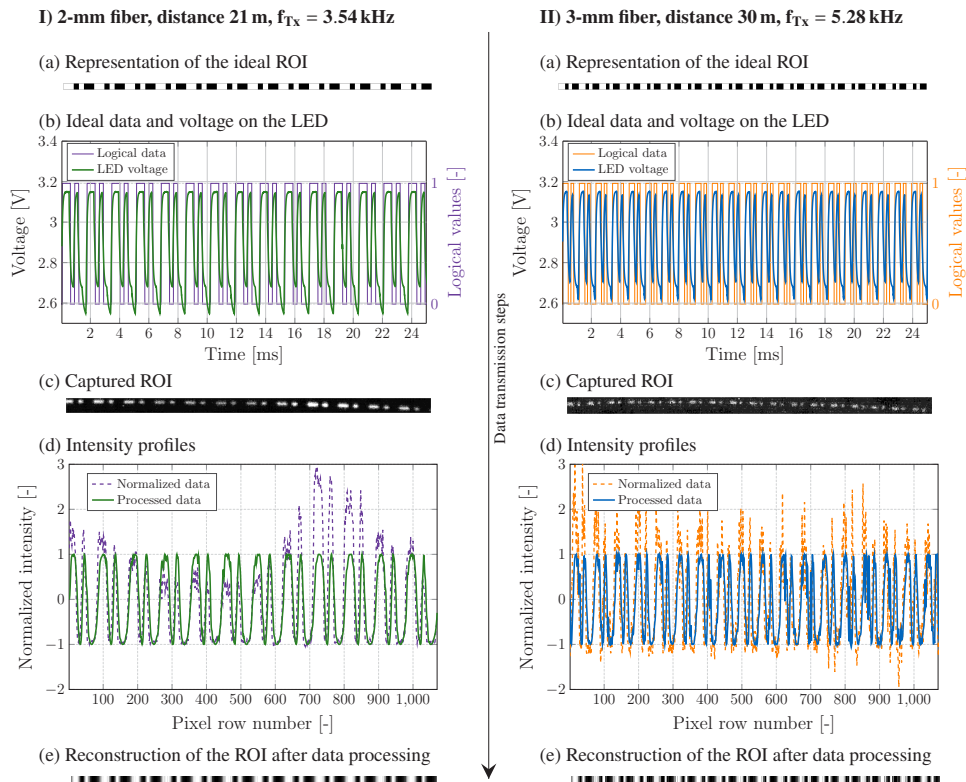
2.2. Data processing

In our experiments, we capture all the data (image frames), and the processing is then carried out in an offline mode. A schematic diagram of the data processing of the captured image frames is shown in Fig. 2. To recover transmitted data, the received image is turned into a grayscale image, and an approximate ROI is found. As the side-emitting fiber might not be perfectly straight in real-case scenarios, the post-processing algorithm is based on peak detection (spots of highest intensity representing logical 1), compensating for slight curvature deviations of the side-emitting fiber. The captured image is cropped and adjusted according to this information. Next, the adjusted image is converted to an intensity profile and preprocessed, which starts with compensation of data trend followed by digital filtration and, finally, equalization, preparing the signal for demodulation. The preprocessing itself is necessary to eliminate distortions from data generation, transmission, and capturing. Compensation of the data trend is necessary due to the exponential decrease of power illuminated from the side-emitting fiber (due to the fiber loss). To counter these differences in illumination we use singular spectrum analysis (SSA) [26], see Fig. 3(c). For digital filtering, we employ an infinite impulse response (IIR) filter as for the limited number of data samples the use of a finite impulse response (FIR) filter would lead to a massive data loss. Before the demodulation, we apply standard matched filtering and finally, we carry out a symbol synchronization.
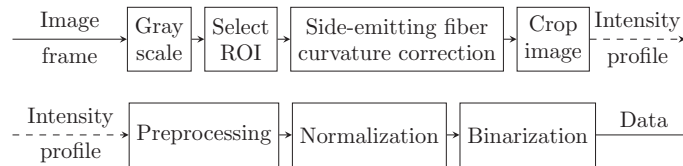
Fig. 2. Schematic diagram of the data processing of captured image frames.

We show, for better illustration, the whole image processing routine, including the signal generation in Fig. 3 on an example of I) a side-emitting fiber with a 2 mm diameter (Fig. 3(I)) at a distance $d = 21$ m and f_{Tx} of 3.54 kHz, and II) a side-emitting fiber with a 3 mm diameter (Fig. 3(II)) at $d = 30$ m and f_{Tx} of 5.28 kHz. The LED is modulated using an on-off-keying (OOK) modulation scheme. Figure 3(a) demonstrates the generated logical data in the form of black and white rectangle-shaped sections along the fiber (the logical zeros and ones), which represents a region of interest (ROI). We aim to showcase an undistorted capture of the ROI, i.e., without distortions from system components or at the LED. Figure 3(a) thus serves as an ideal reference for understanding the outcome in an optimal scenario. Next, Fig. 3(b) shows the ideal logical data compared to the real measured voltage on the LED. We already see some signal distortion given by the LED response. On the camera receiver side, Fig. 3(c) illustrates the captured image already cropped to the selected ROI. Figure 3(d) provides the comparison of the measured and normalized intensity profile and the intensity profile after the processing, when the signal was equalized by the elimination of unwanted peaks. Figure 3(e) shows a reconstruction of the original signal obtained from the image and signal processing of received data. Comparison with the representation of the ideal ROI from Fig. 3(a) shows that the processed signal from

I) 2-mm fiber, distance 21 m, f_{Tx} = 3.54 kHz

(a) Representation of the ideal ROI

(b) Ideal data and voltage on the LED

(c) Captured ROI

(d) Intensity profiles

(e) Reconstruction of the ROI after data processing

II) 3-mm fiber, distance 30 m, f_{Tx} = 5.28 kHz

(a) Representation of the ideal ROI

(b) Ideal data and voltage on the LED

(c) Captured ROI

(d) Intensity profiles

(e) Reconstruction of the ROI after data processing

Fig. 3. Example images I) and II) with parts: (a) Representation of the ideal ROI, (b) ideal logical data and corresponding voltage on the LED, (c) captured ROI, (d) intensity profile of measured and preprocessed data, (e) reconstruction of the ROI after data processing (to show differences with the captured ROI).

Fig. 3(d) matches nicely with the initially generated signal in Fig. 3(b) thus demonstrating reliable performance of the processing algorithm.

When capturing the data, the first captured bit might not be captured completely. That is something that must be taken into consideration when processing the captured image frames. The demodulation itself is then based on matched filtering.

3. Measurements setup

The block diagram of the measurement setup with a photo of the distributed transmitter and the camera receiver side is shown in Fig. 4. An arbitrary waveform generator (Rohde & Schwarz, HMF2550) produced an OOK signal. The data signal was fed to an LED driver (Thorlabs, LEDD1B), which was connected to a white LED (Light Avenue, CW28WP6). Optimal coupling from the LED into the side-emitting fiber was ensured by using a 5D stage consisting of a 3-Axis NanoMax and a pitch and yaw tilt platform (Thorlabs, MAX313D/M and PY003/M). We used side-emitting fibers made of polymethyl methacrylate (PMMA) with outer diameters of 2 mm and 3 mm. A light block was put behind the side-emitting fiber to create the optimal environment for image capture. The side-emitting fiber image was captured by an RS camera placed perpendicularly to the side-emitting fiber with a maximum distance of 40 m. The RS camera was a Raspberry Pi camera module 2 with a Sony IMX219 sensor with a Pentacon auto 50 mm f/1.8 lens.
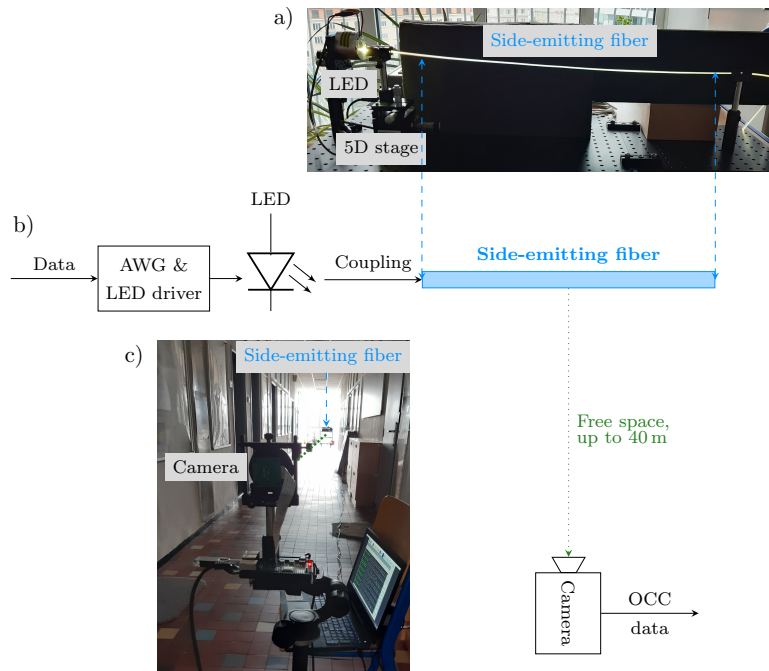
Fig. 4. Measurement setup of the side-emitting fiber-based OCC system: (a) a block diagram of the setup, (b) a close-up photo of the distributed transmitter, and (c) the camera receiver with the side-emitting fiber transmitter in the background.

When preparing the measurement setup, it is important to keep in mind the orientation of the camera's RS with respect to the side-emitting fiber orientation. It is best to keep the side-emitting fiber perpendicular to the RS. However, even when the side-emitting fiber is placed diagonally in the image frame, the system performance should not be negatively affected. Only small deviations of the camera angle by ±10° will have no effect on the OCC performance. In [27], we studied the effect of 0° to 90° bending radius of the side-emitting fiber on the system performance. It was possible to achieve a 100% success of reception (BER below the FEC limit) and we concluded that the bending of the fiber up to 90° does not negatively affect the system performance.

The RS camera resolution was set to a standard Full HD 1920×1080 px with the analog gain G_v of 4. This value was determined as a middle-ground solution for our setup after a series of initial test measurements. The digital gain was equal to 1 to minimize noise increase.

The system was designed to test N_{pps} of 10 pps and 15 pps. To achieve this, Eq. 2 was applied and gave us symbol times $t_{symbol} = 189\,\mu s$ and $282\,\mu s$ and modulation frequencies $f_{Tx} = 5.28$ kHz and 3.54 kHz for $N_{pps} = 10$ pps and 15 pps, respectively. The symbol times t_{symbol} also determine the optimal exposure time, as stated in Eq. 1. For $N_{pps} = 10$ pps, the used exposure time was $t_{exp} = 90\,\mu s$, and for $N_{pps} = 15$ pps it was $t_{exp} = 140\,\mu s$. Data packets of six bits ([010011]) were sent. Note, it is possible to use longer packets with the packet length limit at the half-size of the ROI, otherwise, the packet may not be captured completely [28]. To ensure sufficient amount of data for precise BER calculation, we process multiple packets in each of the 25 captured image frames. This gives us enough processed data that the BER can get as low as $3.7 \cdot 10^{-4}$. If we capture even more image frames, we can lower the BER level and possibly reach even better BER results which we considered not necessary as we were able to safely validate below FEC limit data transmission using our current approach. The list of used equipment, its fundamental parameters, and used variables are provided in Table 1.

Table 1. Equipment, its fundamental parameters, and used variables.

| Parameter	Value
Side-emitting fiber	**ZDEA, Super bright**
Diameter	2 and 3 mm
Fiber to camera distance d	[5, 40] m
LED	**LA CW28WP6**, cold white
Modulation frequencies f_{Tx}	3.54 kHz & 5.28 kHz
Data packet size	6 b/packet [010011]
LED driver	LEDD1B, ThorLabs
Camera Receiver	**Raspberry Pi Camera Module 2**
Lens	Pentacon auto 50 mm f/1.8
Sensor	Sony IMX219
Resolution	1920 × 1080 pixels Full HD
Exposure times t_{exp}	140 µs & 90 µs
Number of pixels per symbol N_{pps}	15 px/symbol & 10 px/symbol

4. Results

The experiment was performed indoors and under ambient light conditions, which according to previous findings [17], does not influence the measurement results. The measurements were carried out for the modulation frequencies f_{Tx} of 3.54 kHz and 5.28 kHz. The side-emitting fiber-camera distance d ranged from 5 m to 40 m with a 1 m step for both side-emitting fibers. A set of 25 image frames was captured at each distance d and frequency f_{Tx}. The captured image frames were processed individually, and the final success of reception (SoR) is their mean value.

Two metrics are used to evaluate the system performance: the SoR and the BER. The limit of well functioning system evaluated by the BER corresponds with the FEC limit, which is $3.8 \cdot 10^{-3}$ [29]. The calculated BER values are displayed in Fig. 5(a) and Fig. 5(b). The frequency $f_{Tx} = 5.28$ kHz for the 2-mm side-emitting fiber follows the FEC limit of $3.8 \cdot 10^{-3}$ up to 30 m and for the 3-mm side-emitting fiber up to 38 m. Moreover, the frequency $f_{Tx} = 3.54$ kHz combined with the 2-mm side-emitting fiber follows the FEC limit up to 35 m and for the 3-mm side-emitting fiber at least up to 40 m. The SoR results are depicted in Fig. 6(a) and Fig. 6(b). Our experimental results at $f_{Tx} = 5.28$ kHz show that for both side-emitting fibers, the SoR was at least 98% up to 40 m distance and at least 99% up to 38 m. For $f_{Tx} = 3.54$ kHz, the SoR was up
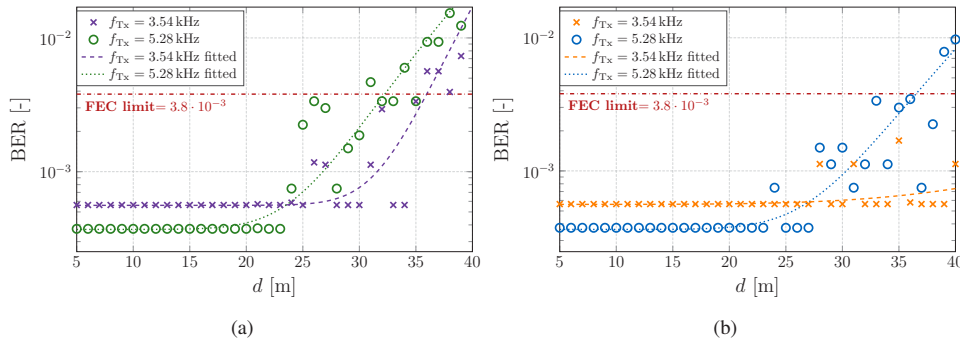
Fig. 5. BER for (a) the 2-mm and (b) the 3-mm side-emitting fiber with marked FEC limit of $3.8 \cdot 10^{-3}$.

to 99% up to 40 m for both side-emitting fiber diameters. Comparing this to the best previously published results in [17] where the SoR of up to 100% was adhered to only up to 0.75 m. Such a significant improvement was mainly due to the improved calculation of f_{Tx} and t_{exp} as we here used the optimal values to minimize inter-symbol interference. More suitable camera settings were also enabled by using a better camera in comparison to previous papers. Enhancement in data processing was ensured by our new algorithm for compensation of the side-emitting fiber curvature. All these modifications lead to an improvement in transmission distance by the above-mentioned two orders.
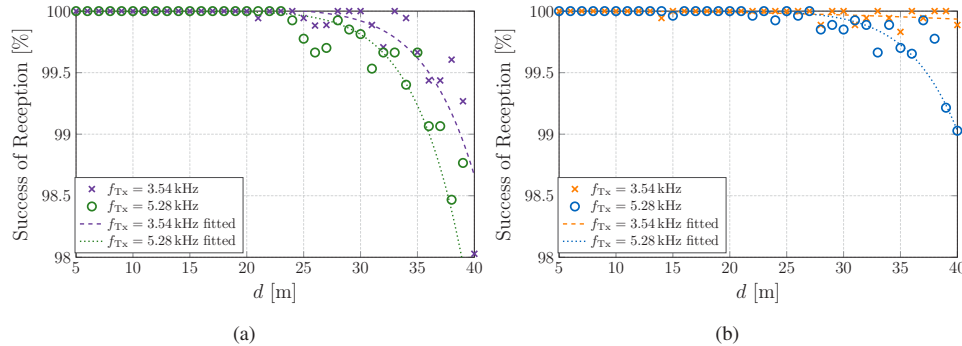
Fig. 6. Success of reception (SoR) for (a) the 2-mm and (b) the 3-mm side-emitting.

From the results, it can be concluded that increasing the fiber diameter just by 1 mm from 2 mm to 3 mm allows us to increase the distance by more than 5 meters for the modulation frequency of 3.54 kHz, as seen in Fig. 6, considering the errors in the SoR. This shows that the redundancy in the columns of region-of-interest, which comes with thicker fiber, helps the demodulation process conducted by the matched filtering. As more image sensor columns are affected by the same illumination, more redundancy is introduced in the system. Thus, the signal-to-noise ratio can increase considerably, which is linked to reduced transmission errors and improved channel performance.

5. Conclusion

This paper demonstrates a new link design approach to optical camera communication using side-emitting fibers as distributed transmitters resulting in more than a two-order link distance increase compared to previous works.

We demonstrated the importance of the LED modulation frequency dependence and the corresponding RS camera exposure time on the minimization of the inter-symbol interference. As a practical demonstration, we selected two modulation frequencies, 3.54 kHz and 5.28 kHz, giving us exposure times of 140 μs and 90 μs resulting in 15 and 10 pixels per symbol at the rolling shutter camera, respectively.

In terms of the success of reception, with the 2-mm side-emitting fiber, the measurement results provide at least 98% success of reception for up to 40 m distance, whereas, with the 3-mm side-emitting fiber, the success of reception was at least 99% up to 40 m distance. When discussing BER and the $3.8 \cdot 10^{-3}$ FEC limit for the 2-mm side-emitting fiber, the FEC limit adhered up to 30 m for 5.28 kHz and up to 35 m for 3.54 kHz. For the 3-mm side-emitting fiber, the FEC limit has been met up to 38 m for 5.28 kHz and up to 40 m for 3.54 kHz.

The proposed OCC system using side-emitting fiber as a distributed transmitter has shown highly-reliable long-distance indoor coverage. The modulation frequency of 5.28 kHz offers

various indoor sensory applications. With the cost of lower modulation frequency and, thus, the data rate, the proposed side-emitting fiber-based OCC system might be stretched into even longer transmission distances, possibly also promising for mid-/long-range outdoor OCC links. In future experiments, we plan to improve the system by using real data clustered in longer packets with the 6-bit packet headers that we used in this paper.

Disclosures. The authors declare no conflicts of interest.

Data availability. Data underlying the results presented in this paper are not publicly available at this time but may be obtained from the authors upon reasonable request.

References

1. T. Tripp, A. S. Hamza, B. Underwood, and R. Tashakkori, "Low-cost UFSOOK-based optical camera communication link for IoT applications," in *6th World Forum on Internet of Things* (IEEE, 2020).
2. V. Matus, V. Guerra, C. Jurado-Verdu, S. Zvanovec, J. Rabadan, and R. Perez-Jimenez, "Design and implementation of an optical camera communication system for wireless sensor networking in farming fields," in *32nd Annual International Symposium on Personal, Indoor and Mobile Radio Communications* (IEEE, 2021).
3. V. P. Rachim and W.-Y. Chung, "Multilevel intensity-modulation for rolling shutter-based optical camera communication," IEEE Photonics Technol. Lett. **30**(10), 903–906 (2018).
4. P. Luo, M. Zhang, Z. Ghassemlooy, H. L. Minh, H.-M. Tsai, X. Tang, L. C. Png, and D. Han, "Experimental demonstration of RGB LED-based optical camera communications," IEEE Photonics J. **7**(5), 1–12 (2015).
5. A. Islam, M. T. Hossan, and Y. M. Jang, "Convolutional neural networkscheme–based optical camera communication system for intelligent internet of vehicles," Int. J. Distributed Sens. Networks **14**(4), 155014771877015 (2018).
6. E. Eso, S. Teli, N. B. Hassan, S. Vitek, Z. Ghassemlooy, and S. Zvanovec, "400 m rolling-shutter-based optical camera communications link," Opt. Lett. **45**(5), 1059 (2020).
7. K. Jiang, X. Chi, F. Ji, and S. Li, "Research on mobile phone swaying and receiving position in optical camera communication," Optoelectron. Lett. **18**(2), 85–90 (2022).
8. V. Georlette, F. Piras, C. Jurado-Verdu, S. Bette, N. Point, and V. Moevaert, "Content triggering system using tricolor LED strips and optical camera communication in rolling shutter mode," in *Third South American Colloquium on Visible Light Communications* (IEEE, 2021).
9. V. Matus, E. Eso, S. R. Teli, R. Perez-Jimenez, and S. Zvanovec, "Experimentally derived feasibility of optical camera communications under turbulence and fog conditions," Sensors **20**(3), 757 (2020).
10. A. Reupert, J. Schröder, and L. Wondraczek, "Radiation from side-emitting optical fibers and fiber fabrics: Radiometric model and experimental validation," Adv. Photonics Res. **3**(4), 2100104 (2022).
11. S. L. Logunov, K. W. Bennett, E. J. Fewkes, W. S. Klubben, and M. Paniccia, "Silica nano-structured fiber for illumination," J. Lightwave Technol. **37**(22), 5667–5673 (2019).
12. M. Lanzarini-Lopes, S. Garcia-Segura, K. Hristovski, M. Messerly, A. J. Simon, and P. Westerhoff, "Particle-modified polymeric cladding on glass optical fibers enhances radial light scattering," J. Opt. Soc. Am. B **36**(6), 1623 (2019).
13. W. S. Klubben, S. L. Logunov, E. J. Fewkes, J. Mooney, P. M. Then, P. G. Wigley, H. Schreiber, K. Matias, C. J. Wilson, and M. Ocampo, "Novel light diffusing fiber for use in medical applications," in *SPIE Proceedings*, I. Gannot, ed. (SPIE, 2016).
14. B. Selm, E. A. Gürel, M. Rothmaier, R. M. Rossi, and L. J. Scherer, "Polymeric optical fiber fabrics for illumination and sensorial applications in textiles," J. Intell. Mater. Syst. Struct. **21**(11), 1061–1071 (2010).
15. C. Jurado-Verdu, V. Guerra, V. Matus, C. Almeida, and J. Rabadan, "Optical camera communication as an enabling technology for microalgae cultivation," Sensors **21**(5), 1621 (2021).
16. L. Liu, S. Chen, and L.-K. Chen, "Optical camera communication using plastic fiber array for spatial multiplexing," in *Photonics Conference* (IEEE, 2022).
17. S. R. Teli, K. Eollosova, S. Zvanovec, Z. Ghassemlooy, and M. Komanec, "Optical camera communications link using an LED-coupled illuminating optical fiber," Opt. Lett. **46**(11), 2622 (2021).
18. S. R. Teli, K. Eollosova, S. Zvanovec, Z. Ghassemlooy, and M. Komanec., "Experimental Characterization of Fiber Optic Lighting - Optical Camera Communications," in *32nd Annual International Symposium on Personal, Indoor and Mobile Radio Communications* (IEEE, 2021), pp. 1–5.
19. D.-C. Tsai, Y.-H. Chang, C.-W. Chow, Y. Liu, C.-H. Yeh, C.-W. Peng, and L.-S. Hsu, "Optical camera communication (OCC) using a laser-diode coupled optical-diffusing fiber (ODF) and rolling shutter image sensor," Opt. Express **30**(1), 1 (2022).
20. Y.-H. Chang, S.-Y. Tsai, C.-W. Chow, C.-C. Wang, D.-C. Tsai, Y. Liu, and C.-H. Yeh, "Unmanned-aerial-vehicle based optical camera communication system using light-diffusing fiber and rolling-shutter image-sensor," Opt. Express **31**(11), 18670 (2023).
21. P. Imperatore, G. Testa, G. Persichetti, and R. Bernini, "Power coupling between light diffusing fibers: Modelling and validation," J. Lightwave Technol. **40**(3), 813–821 (2022).

22. C. Jurado-Verdu, V. Guerra, V. Matus, J. Rabadan, and R. Perez-Jimenez, "Convolutional autoencoder for exposure effects equalization and noise mitigation in optical camera communication," Opt. Express **29**(15), 22973 (2021).

23. X. Li, N. B. Hassan, A. Burton, Z. Ghassemlooy, S. Zvanovec, and R. Perez-Jimenez, "A Simplified Model for the Rolling Shutter Based Camera in Optical Camera Communications," in *15th International Conference on Telecommunications* (IEEE, 2019), pp. 1–5.

24. V. Matus, V. Guerra, S. Zvanovec, J. Rabadan, and R. Perez-Jimenez, "Sandstorm effect on experimental optical camera communication," Appl. Opt. **60**(1), 75–82 (2021).

25. V. Matus, V. Guerra, C. Jurado-Verdu, S. R. Teli, S. Zvanovec, J. Rabadan, and R. Perez-Jimenez, "Experimental evaluation of an analog gain optimization algorithm in optical camera communications," in *12th International Symposium on Communication Systems, Networks and Digital Signal Processing* (IEEE, 2020).

26. N. Golyandina and A. Zhigljavsky, *Singular Spectrum Analysis for Time Series* (Springer Berlin Heidelberg, 2013).

27. K. Eollosova, S. R. Teli, S. Zvanovec, Z. Ghassemlooy, R. Perez-Jimenez, and M. Komanec, "Towards optical camera communications using a shape-tailored illuminating optical fiber," in *13th International Symposium on Communication Systems, Networks and Digital Signal Processing* (IEEE, 2022).

28. C. Jurado-Verdu, V. Guerra, J. Rabadan, R. Perez-Jimenez, and P. Chavez-Burbano, "RGB synchronous VLC modulation scheme for OCC," in *11th International Symposium on Communication Systems, Networks & Digital Signal Processing* (IEEE, 2018).

29. T. Mizuochi, *Forward Error Correction* (Springer Berlin Heidelberg, 2010), vol. 6, pp. 303–333.